Vehicle-to-Vehicle Channel Models with Large Vehicle Obstructions

Ruisi He[†‡], Andreas F. Molisch[‡], Fredrik Tufvesson[♯], Zhangdui Zhong[†], Bo Ai[†], and Tingting Zhang[§‡]
[†]State Key Laboratory of Rail Traffic Control and Safety, Beijing Jiaotong University, Beijing, China
[‡]Department of Electrical Engineering, University of Southern California, Los Angeles, USA
[♯]Department of Electrical and Information Technology, Lund University, Lund, Sweden
[§]Harbin Institute of Technology, Shenzhen Graduate School, Shenzhen, Guangdong, China
Email: ruisi.he@ieee.org

***Abstract*—Vehicle-to-Vehicle (V2V) communication is an enabler for improved traffic safety and congestion control. As for any wireless system the ultimate performance limit is determined by the propagation channel. A particular point of interest is the shadowing effect of large vehicles such as trucks and buses, as this might affect the communication range significantly. In this paper we present measurement results and model the propagation channel in which a bus acts as a shadowing object between two passenger cars. The measurement setup is based on a WARP FPGA software radio as transmitter, and a Tektronix RSA5106A real-time complex spectrum analyzer as receiver. We analyze the influence of the bus location and car separation distance on the large-scale path loss, shadowing, and small-scale fading. The main effect of the bus is that it is acting as an obstruction creating an additional 15-20 dB attenuation. A Nakagami distribution is found to describe the statistics of the small-scale fading, by using Akaike's Information Criterion and the Kolmogorov-Smirnov test. The distance-dependency of the path loss is analyzed, and a stochastic model is developed to reflect the impact.**

***Index Terms*—Large vehicle obstructions, vehicle-to-vehicle, path loss, shadow fading, small-scale fading.**

I. Introduction

RESEARCH into vehicle-to-vehicle (V2V) wireless communications has recently attracted much interest due to its wide application in the field of Intelligent Transportation Systems (ITS). Acquiring information through on-car sensors, and exchanging it with neighbors through wireless vehicular ad-hoc networks (VANETs), allows each of the involved cars to have more detailed knowledge of the surrounding traffic situation, which in turn can help to improve safety and reduce traffic congestion.

It is well-known that the design of a wireless system requires a deep understanding of the propagation channels. However, even though many V2V measurement campaigns have been conducted over the past few years, see the overviews [1], [2] and references therein, there is still a lack of results regarding many important channel characteristics. One important topic is to explore the impact of vehicles between the TX and RX in V2V links, which may lead to shadowing of the transmitted signal and extra delay spread. The relatively low heights of the antennas (mostly below 2 m) in V2V communication imply that the line-of-sight (LOS) can easily be blocked by other vehicles between the TX and RX [3], especially some large vehicles like buses and trucks. The importance of shadowing by other vehicles was analyzed in [4], but many results for V2V channels do not distinguish between LOS and non-LOS (NLOS) conditions; rather, all channel samples are lumped together in the analysis [1]. This approach not only limits the accuracy of the channel models, but also results that almost all of the vehicular Ad Hoc networks (VANET) simulators neglect the impact of vehicles as obstacles on propagation, which is mainly due to the lack of an appropriate methodology capable of incorporating the effect of vehicles [3] [5]. It is necessary and important to explore the impact of large vehicles between the TX and RX in V2V links.

Recently, some experimental work about large vehicle obstructions have been conducted. In [4] and [6] channel measurements including the vehicle obstruction scenarios in urban and highway environments are conducted, however, the NLOS cases caused by the vehicles in [4] and [6] either include the effect of the small cars and vans, or occur intermittently in the measurements. In [3] and [7] the effect of the trucks and vans on the received signal strength indicator is investigated. However, most of the measurements are conducted at several separate locations, so that the discontinuous (with respect to distance) sampling complicates a detailed and accurate analysis of shadow fading, and the distance-dependence of some channel parameters. To alleviate these limitations, this paper presents a detailed analysis of the impact of a large-vehicle obstructions based on the results from an extensive measurement campaign on campus of University of Southern California (USC), Los Angeles, USA. In our measurements, the received signal is sampled continuously, by using a self-designed trigger system, at a rate enabling dynamic measurements of both the small-scale fading, and analyzing how the channel parameters depend on vehicle location and TX and RX separation distance. Note that as the model is based on measurements, it is thus limited to the measurement conditions. Some extended analysis and a detailed discussion of the model range are presented in [8].

The remainder of the paper is organized as follows: Section II describes our measurement campaign for NLOS V2V channels, where the LOS between two passenger cars is blocked by a school bus. Section III presents the models for the path loss and shadow fading. Section IV analyzes the small-scale fading behavior, whereas Section V concludes the paper.

978-1-4799-2003-7/14/$31.00 ©2014 IEEE

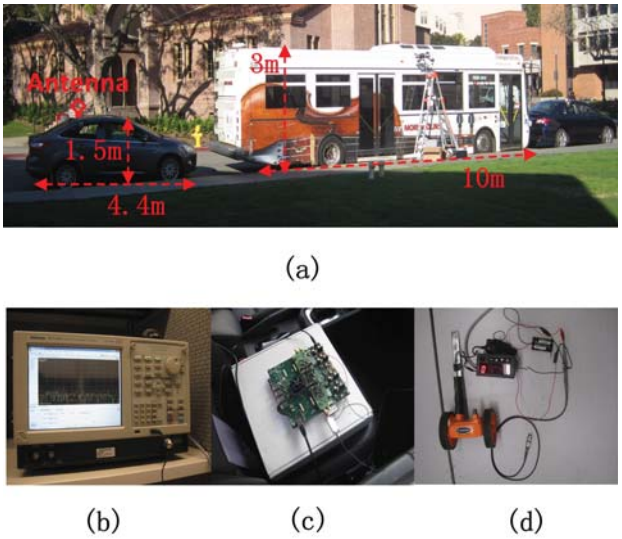

Fig. 1. V2V measurement setup. (a) School bus and compact cars; (b) Tektronix RSA5106A real-time spectrum analyzer; (c) WARP FPGA board; (d) Self-designed trigger wheel.

TABLE I
MEASURED V2V LINKS (CC - CAR-TO-CAR)

Propagation Link	Bus Location	d_2 (m)
CC-A1	A	0.1
CC-A2	A	50
CC-B1	B	0.1
CC-B2	B	50

II. MEASUREMENT CAMPAIGN

A. Measurement System

We use a measurement system using software radio units, the WARP FPGA boards [9], as transmitters. The baseband transmitted signal has a 15 MHz bandwidth, larger than the 10 MHz bandwidth of 802.11p [2]. The transmit signal is a Zadoff-Chu sequence, which provides almost-constant magnitude in the frequency domain and a small peak-to-average-ratio in the time domain [10]. In the frequency domain the signal is defined as

$$X(m) = e^{j\pi m(m+1)/M_{zc}} \tag{1}$$

where $0 \leq m \leq M_{zc} - 1$ and $M_{zc} = 2^{10}$ is the length of the sequence.

We up convert the base band signal to a 5.805 GHz carrier frequency. The measured band is free from interference, as confirmed by measurements with a spectrum analyzer. A Shireen high performance 5.8 GHz amplifier is connected to the WARP board and provides a transmit output power of 28 dBm. The receiver has a 23 dB low-noise amplifier JCA04-239, which is connected to a Tektronix RSA5106A real-time complex spectrum analyzer. Both the transmitter and the receiver use 25 cm long L-com HG2458MGRD-RSP omnidirectional antennas. In the measurements, the TX is set to transmit continuously. The RX is connected to a trigger wheel, and saves a snapshot of the transfer function every 0.5 wavelength (≈2.5 cm). The measurement system is shown in Fig. 1. Since the quantity of interest for this campaign was signal power, the synchronization of TX to RX did not have a major impact on our results.

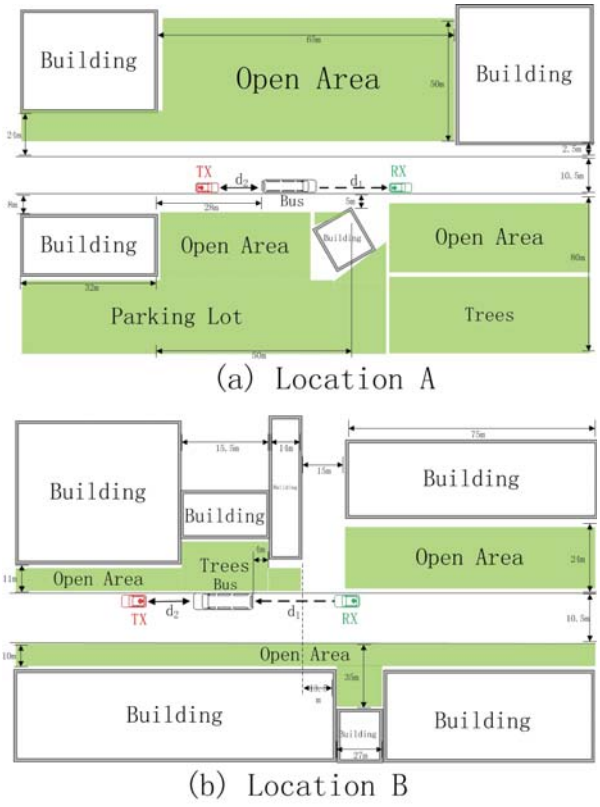

Fig. 2. Overview of the measurement locations.

B. Measurement Scenarios

The measurements are conducted on a street on the campus of University of Southern California using a standard American school bus and two compact cars. In our NLOS measurements, we parked the school bus in two different locations as shown in Fig. 2. The bus is parked between the two cars and kept stationary in the measurements. In location A, the bus is parked in an open area, and there are no buildings close to the bus; in location B, there are high buildings on both sides of the street. We park the car with the TX at a fixed distance d_2 on one side of the bus, and we move the car with the RX along d_1 on the other side. The TX/RX antennas are placed on the roof of each car, 1.2 m in front of the back end of the car, as shown in Fig. 1

In the measurements, the speed of the car is generally less than 1 m/s. The bus is 10.0 m long and 3.0 m high, and the compact cars are 4.4 m long and 1.5 m high. Table I summarizes the details and abbreviations of all the car-to-car (CC) propagation links.

III. PATH LOSS AND SHADOW FADING

The local path gain is determined from the measured transfer functions $H(d, f_l)$ as:

$$PG(d) = \frac{1}{N_f}\left(\sum_{l=1}^{N_f} (H(d, f_l))^2\right) \tag{2}$$

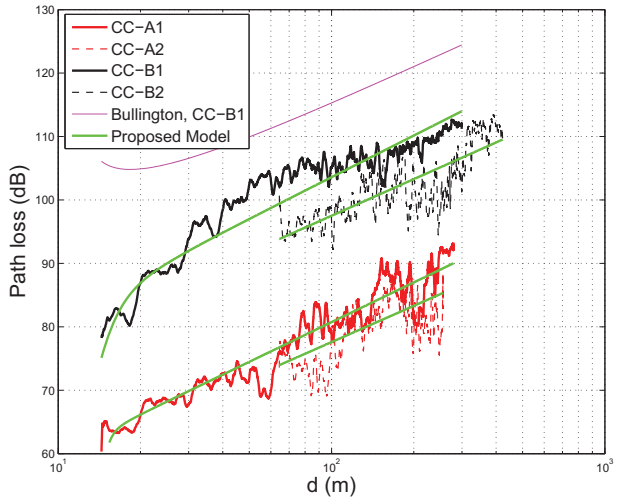

Fig. 3. NLOS path loss as a function of the separation distance. For clarity, the results in CC-A are plotted with a -20 dB vertical offset. A double knife-edge diffraction model based on the Bullington's method for CC-B1 is plotted for comparison.

where $N_f = 385$ is the number of measured frequency points. To remove the effect of small-scale fading, we use in this paper a sliding window of length 40 wavelengths. This provides an estimate of the combined pathloss/shadowing, which is then analyzed as a function of the separation distance d between TX and RX antennas. The lowest average signal-to-noise-ratio (SNR) measured at large distance is approximately 15 dB. At most locations, the SNR is larger than 20 dB so that an accurate estimation of channel parameters is possible.

A. General Observations

The measured pathloss/shadowing in the NLOS scenarios are plotted in Fig. 3. Several observations are worth noting:

1) The path loss in the NLOS scenario is generally 15-20 dB higher compared with the results of the LOS measurements in [11]. The additional loss is higher than the 9-10 dB reported in [4]. Note that the obstruction loss in [4] is an averaged result over the impact of obstructions by mainly other cars and typically with a larger distance to the obstructing object than here. By conducting the particular measurements, we find that the large vehicle obstruction leads to larger losses than reported before.

2) In the NLOS measurements, for a fixed d, a smaller d_2 leads to a larger path loss. This can be readily explained by the physics of diffraction and shadowing: diffraction losses increase when d_2 decreases. However, traditional path loss models, e.g., the log-distance model $PL \propto d^{-n}$, does not reflect this phenomenon.

3) For the NLOS-CC-B1 link, a dual-slope path loss model with a breakpoint should be used; while for the other three curves, a single slope model generally works well.

4) Ref. [12] suggests that the double knife-edge diffraction model is a good approximation for the additional attenuation caused by the large vehicle obstructions. However, Fig. 3 shows that the double knife-edge diffraction model based on the Bullington's method [10] fails to provide a good fit. This is because in a typical street, usually more multipath components are received by reflections/scatterings from the scatterers around the street, which means the ideal double knife-edge diffraction propagation does not occur.

The above observations show that in the NLOS scenarios, an electromagnetic analysis of diffraction by a simple-shaped object cannot provide sufficient accuracy because the randomly distributed scatterers in the street also have significant effects. A suitable statistical path loss model for the V2V NLOS cases should be able to reflect the individual effect of d_1 and d_2.

B. Path Loss Modeling

To model the path loss in the NLOS scenarios, we propose a model with two different types of distance dependence. The first term follows the "classical" power-law path loss model d^{-n_1}, i.e., $(d_1 + d_2 + L_{\mathrm{Bus}} + L_{\mathrm{Car}})^{-n_1}$, where L_{Bus} and L_{Car} are the lengths of the bus and the cars, and n_1 is the associated path loss exponent. The second term represents the diffraction of the bus, which is affected by the distance between the TX and the bus. We therefore introduce a factor of $(d_1 d_2)^{-n_2}$. Note that while this model is inspired by the physics of the propagation, it is a heuristic, whose ultimate justification lies in its ability to fit the measurement data.

To summarize, the path gain covering the effect of the large vehicle obstructions is modeled as

$$PG = PG_1 + PG_2 = \frac{G_1}{(d)^{n_1}} + \frac{G_2}{(d_1 d_2)^{n_2}} \qquad (3)$$

where n_1 and n_2 are the equivalent path loss exponents. G_1 and G_2 are the reference levels for the gains. By using a least mean square error (LMSE) regression fit on the logarithm of the measured path gains, we obtain the G_1, G_2, n_1, and n_2. Note that Eq. (3) has too many degrees of freedom. Therefore, to ensure a reasonable fit and sufficient accuracy, we add some limitations to the range of the estimated parameters when we do the LMSE regression fit as follows: $1.5 \leq n_1 \leq 3$, $3 \leq n_2 \leq 8$, and $0.001 \leq G_1/G_2 \leq 1000$. The above limitations are used to ensure that the estimated parameters follow the physical insights. Table II summarizes the estimated parameters. From the table, we find that the estimated n_1 is around 2 and the estimated n_2 is around 4. We note that placing the TX far from the bus (CC-A2 and CC-B2 links) results in a smaller value of G_2, i.e., the term of $(d_1 d_2)^{-n_2}$ plays a smaller role. We can see that in the CC-A1 and CC-A2 links, the values of G_2 are generally larger than in the CC-B1 and CC-B2 links. This means that the diffraction has a more important role when the bus is located in an open area, because in this case there is no scatterers around to reflect the paths to the receiver.

To evaluate the goodness of the regression line we study the coefficient of determination, R^2. It is given by

$$R^2 = \left(\sum_{i=1}^{N} w_i (\hat{y}_i - \bar{y})^2 \right) \Big/ \left(\sum_{i=1}^{N} w_i (y_i - \bar{y})^2 \right) \qquad (4)$$

where y_i and $\hat{y}_i$ are the measured signals and the estimate in dB, respectively. $\bar{y}$ is the mean value of the measured signals, w_i denotes the weight and is chosen as $w_i = 1/N$. R^2 ranges

TABLE II
PARAMETERS OF THE PATH LOSS AND SHADOW FADING MODELS

Scenario	G_1	G_2	n_1	n_2	R^2	σ_S (dB)	d_{cor} (m)
CC-A1	1.22×10^{-6}	6.36×10^{-6}	2.08	4.02	0.85	2.86	6.73
CC-A2	1.10×10^{-6}	2.02×10^{-6}	1.90	3.97	0.77	3.50	10.72
CC-B1	1.00×10^{-6}	4.76×10^{-6}	2.18	3.82	0.88	2.79	6.70
CC-B2	1.23×10^{-6}	1.17×10^{-6}	1.92	3.91	0.80	3.30	5.46

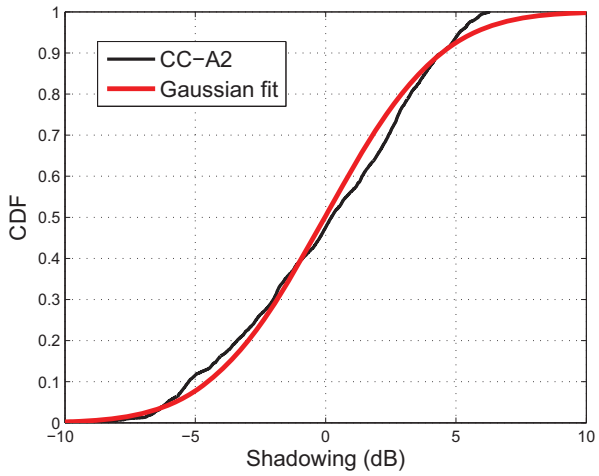

Fig. 4. Example plot of the shadow fading CDF on dB scale together with a maximum likelihood estimate of the Gaussian distribution.

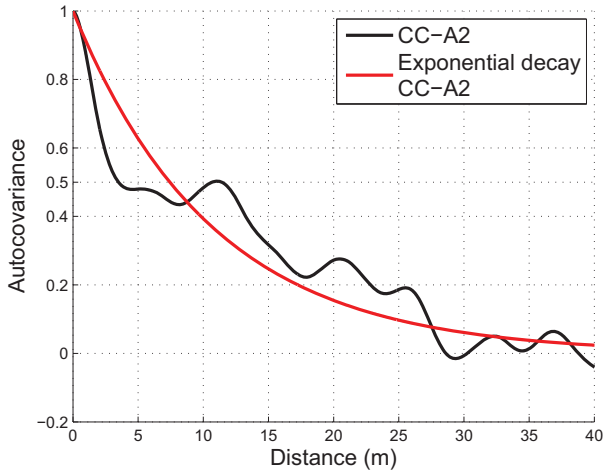

Fig. 5. Example plot of the spatial autocovariance of shadowing together with an exponential decay function.

from 0 to 1, with a value closer to 1 indicating that the regression model fits the data better. From Table II we can see that the R^2 is larger than 0.75 for all NLOS cases, which means a good fit. Fig. 3 shows the proposed model together with the measurements. Note that we use path loss in Fig. 3, which is the inverse of the path gain.

C. Shadow Fading

We remove the distance-dependence by using the above proposed model from the measured path loss, and analyze the deviation from this, which we denote as shadowing gain X_σ. Shadow fading on a dB scale is conventionally modeled as a zero-mean Gaussian process [10] (i.e., it follows a Lognormal distribution on a linear scale), with a standard deviation of σ_S. Fig. 4 shows an example plot of the cumulative distribution function (CDF) of the measured shadowing gain for the NLOS-CC-A2 link. Table II summarizes the measured σ_S. We find that the standard deviation of the shadowing gain varies in the similar range as reported in previous work, e.g., for the measured urban LOS scenarios in [11] $\sigma_S = 1.7$ dB was reported while in [13] $\sigma_S = 3.4$ dB.

Moreover, we study the autocorrelation of the shadow fading by using the spatial autocovariance, expressed as

$$r(\Delta d) = \frac{E\{[X_\sigma(d) - E(X_\sigma(d))][X_\sigma(d+\Delta d) - E(X_\sigma(d+\Delta d))]\}}{\sqrt{\mathrm{Var}[X_\sigma(d)]}\sqrt{\mathrm{Var}[X_\sigma(d+\Delta d)]}} \quad (5)$$

where d is the distance and Δd is the separation distance. $E[\cdot]$ and $\mathrm{Var}[\cdot]$ denote the expected value and the variance of $[\cdot]$ respectively. For cellular channels it has been suggested [14] that $r(\Delta d)$ can be modeled using an exponential decay function, expressed as

$$r(\Delta d) = \exp(-\frac{|\Delta d|}{d_{\mathrm{cor}}}) \quad (6)$$

where d_{cor} represents the decorrelation distance, here it corresponds to the distance at which the autocorrelation drops to 0.5. An example plot of the autocovariance are shown in Fig. 5. It can be observed from the figure that the estimated autocovariance curve can be approximated as an exponential decay function. The measured d_{cor}'s are summarized in Table II. We can see that d_{cor} for a wide range of NLOS links (NLOS-CC-A1, -B1, -B2) are similar and consistent with the urban measurements in [4]. A high d_{cor} is observed in the NLOS-CC-A2 link, which may be explained by the large d_2 and the relative open surrounding environment for this link.

IV. SMALL-SCALE FADING

After removing the path loss and the shadow fading from the raw data using a sliding window of length 40 wavelengths, we use all the measured space/frequency points within a 40 wavelengths window to investigate the small-scale fading behavior.

A. Amplitude Distribution

We first examine the empirical distribution of the received amplitudes by using the Akaike Information Criteria (AIC)

TABLE III
BEST FIT RATE OF THE SMALL-SCALE FADING BASED ON THE AIC AND KS TESTS

Distribution	Ricean		Nakagami		Rayleigh		Weibull	
Scenario	AIC	KS	AIC	KS	AIC	KS	AIC	KS
CC-A1	8.22%	71.18%	47.88%	83.69%	0.47%	41.91%	43.42%	82.83%
CC-A2	30.51%	86.96%	40.36%	85.26%	0.58%	37.74%	28.54%	84.86%
CC-B1	20.94%	88.74%	20.85%	87.70%	1.53%	67.70%	56.67%	91.29%
CC-B2	18.71%	78.40%	34.90%	80.94%	0.55%	38.17%	45.84%	81.31%
Overall	18.81%	81.93%	35.34%	84.10%	0.79%	46.65%	45.06%	84.88%

[15], which includes a tradeoff between underfitting and overfitting the model, and has been widely used in the selection of suitable distribution functions [16]. The AIC can only suggest the best model from a set of candidate models. We therefore select four widely used small-scale fading distributions as the candidates [1] [2]: Ricean, Rayleigh, Nakagami, and Weibull distributions. All the above distributions have been widely used in the V2V scenarios, however, often an analysis of the most suitable distributions is neglected. The AIC for the j-th candidate distribution that has a probability density function $g_{\hat{\theta}_j}$ given by

$$\mathrm{AIC}_j = -2\sum_{n=1}^{N} \log_e[g_{\hat{\theta}_j}(x_n)] + 2U \tag{7}$$

where g is the probability density function (PDF) of the candidate distribution, $\hat{\theta}_j$ is the maximum likelihood estimate of the distribution parameter vector θ_j obtained from the measurements, and U is the dimension of vector $\hat{\theta}_j$. N is the size of sample set $x = x_1, x_2 \cdots x_N$. For convenience, we define the Akaike weights w_j as [16]

$$w_j = \frac{\exp(-\Phi_j/2)}{\sum_{i=1}^{J}\exp(-\Phi_i/2)} \tag{8}$$

where $\Phi_j = \mathrm{AIC}_j - \min_i(\mathrm{AIC}_i)$, and $\min_i \mathrm{AIC}_i$ denotes the minimum AIC value over all J candidate families. The model with the highest Akaike weight is the best distribution to describe the data set.

We use a sliding/overlapped 40 wavelengths window to estimate the small-scale fading distribution. Fig. 6 shows an example plot of the Akaike weights for the CC-A1 link. Table III summarizes the relative frequency of AIC selecting each of the candidate distributions as best fit. Several observations in this comparison are worth noting:

1) A Weibull distribution shows the best fit in the NLOS scenarios for over 45%, which has also been suggested in [17]; while the Nakagami distribution also indicates a reasonable fit with a best fit rate of 35.34%, which is consistent with the results in [18]. The Ricean distribution only has a best fit rate of 18.81% in the NLOS scenarios.

2) A Rayleigh distribution does not provide the best fit in the V2V NLOS scenarios.

It is noteworthy that there is no mechanism available of using AIC to guarantee the chosen model will provide an adequate fit to the data. Therefore, a Kolmogorov-Smirnov (KS) test with a 95% confidence interval is applied to all

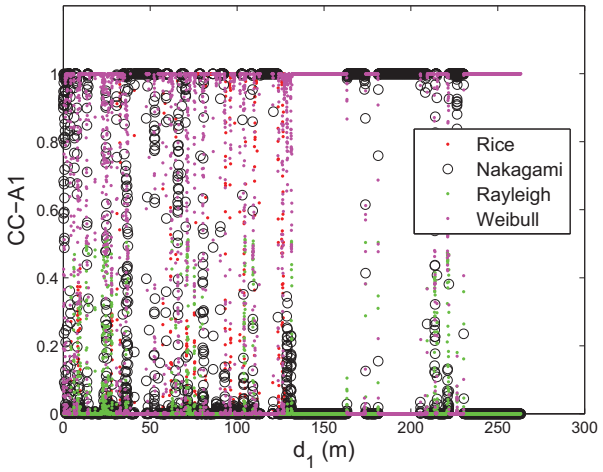

Fig. 6. Akaike weights for the four candidate distributions in V2V CC-A1 link.

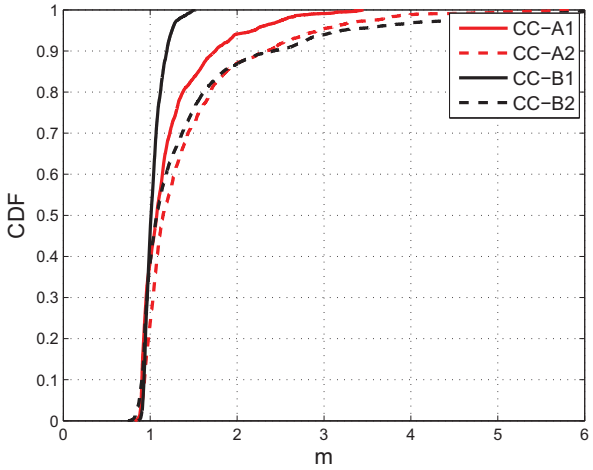

Fig. 7. CDF of the shape factor m in the V2V scenarios.

the candidate families to ensure that a satisfactory fit is obtained. The passing rate for different distribution functions are tabulated in Table III. Generally, the Weibull distribution has the highest passing rate, but the Nakagami and Ricean distributions also show reasonable passing rates. For the Nakagami distribution, the passing rate of 84.1% verifies that it offers a satisfactory fit. An advantage of the Nakagami distribution is that it can be treated more easily than Weibull in theoretical investigations, and a number of papers have investigated generating (possibly correlated) Nakagami distributions,

TABLE IV
STATISTICS OF THE SHAPE FACTOR m IN THE MEASURED SCENARIOS

m	Mean	Std	50%	90%
CC-A1	1.22	0.42	1.08	1.75
CC-A2	1.43	0.71	1.15	2.33
CC-B1	1.04	0.11	1.01	1.19
CC-B2	1.42	0.89	1.07	2.42
Overall	1.27	0.65	1.06	1.82

see [19] [20] and references therein. For this reason, and since both Weibull and Nakagami provide good fits, we henceforth use the Nakagami distribution.

B. Nakagami Distribution

The PDF of the received envelope r is given by

$$p(r; m, \Omega) = \frac{2}{\Gamma(m)} \left(\frac{m}{\Omega}\right)^m r^{2m-1} \exp\left(-\frac{m}{\Omega} r^2\right) \qquad (9)$$

where $\Gamma(\cdot)$ is the Gamma function, Ω is the second moment of the distribution. m is the shape factor that determines the severity of fading - increasing m means decreasing fading depth. A value of $m = 1$ yields the Rayleigh distribution, and $m < 1$ implies more severe fading.

Fig. 7 shows the CDF plots of the shape factor m. We can see that placing the TX close to the bus, i.e., CC-A1 and -B1 cases, leads to a smaller value of m. Table IV summarizes the statistics of the measured m. It is found that the m is generally close to 1 (the Rayleigh distribution) in the NLOS scenarios, which means that the obstruction by the school bus leads to a channel with severe fading.

V. CONCLUSION

Based on a measurement campaign, we presented an analysis of V2V channels when the LOS between the TX and RX is blocked by a large school bus. In the measurements, the channels are sampled continuously by using a trigger system, and the measured data provides a continuous description of the channel behavior over the distance. In our work, the distance between the TX/RX and the school bus, the separation distance between TX and RX, and the surrounding environments are considered in the analysis. It is found that the obstruction by the large school bus generally leads to an additional 15-20 dB attenuation. A Nakagami distribution is suggested to describe the fading statistics based on AIC and KS tests. The distance of the TX/RX to the school bus is found to affect the channel parameters significantly, and a stochastic model is presented to reflect the impact. The results show the effect of large vehicle obstructions in V2V scenarios, and can thus be applied to the VANETs design and development of a channel simulator.

VI. ACKNOWLEDGMENTS

The work is supported by the National Science Foundation Major Research Infrastructure (MRI) program, the Key grant Project of Chinese Ministry of Education (No.313006), the National Natural Science Foundation of China under Grant 61222105, the Beijing Municipal Natural Science Foundation under Grant 4112048, and the Fundamental Research Funds for the Central Universities under Grant 2010JBZ008.

REFERENCES

[1] A. Molisch, F. Tufvesson, J. Karedal, and C. Mecklenbrauker, "A survey on vehicle-to-vehicle propagation channels," *Wireless Communications, IEEE*, vol. 16, no. 6, pp. 12–22, 2009.

[2] C. F. Mecklenbrauker, A. F. Molisch, J. Karedal, F. Tufvesson, A. Paier, L. Bernado, T. Zemen, O. Klemp, and N. Czink, "Vehicular channel characterization and its implications for wireless system design and performance," *Proceedings of the IEEE*, vol. 99, no. 7, pp. 1189–1212, 2011.

[3] R. Meireles, M. Boban, P. Steenkiste, O. Tonguz, and J. Barros, "Experimental study on the impact of vehicular obstructions in VANETs," in *Vehicular Networking Conference (VNC), 2010 IEEE*. IEEE, 2010, pp. 338–345.

[4] T. Abbas, F. Tufvesson, K. Sjöberg, and J. Karedal, "Measurement based shadow fading model for vehicle-to-vehicle network simulations," *arXiv preprint arXiv:1203.3370*, 2012.

[5] S. Biddlestone, K. Redmill, R. Miucic, and Ü. Özgüner, "An integrated 802.11 p WAVE DSRC and vehicle traffic simulator with experimentally validated urban (LOS and NLOS) propagation models," *Intelligent Transportation Systems, IEEE Transactions on*, vol. 13, no. 4, pp. 1792–1802, 2012.

[6] L. Bernadó, T. Zemen, F. Tufvesson, A. F. Molisch, and C. F. Mecklenbräuker, "Delay and Doppler spreads of non-stationary vehicular channels for safety relevant scenarios," *arXiv preprint arXiv:1305.3376*, 2013.

[7] M. Boban, R. Meireles, J. Barros, O. Tonguz, and P. Steenkiste, "Exploiting the height of vehicles in vehicular communication," in *Vehicular Networking Conference (VNC), 2011 IEEE*. IEEE, 2011, pp. 163–170.

[8] R. He, A. F. Molisch, F. Tufvesson, Z. Zhong, B. Ai, and T. Zhang, "Vehicle-to-vehicle propagation models with large vehicle obstructions," *Intelligent Transportation Systems, IEEE Transactions on*, under review.

[9] K. Amiri, Y. Sun, P. Murphy, C. Hunter, J. R. Cavallaro, and A. Sabharwal, "Warp, a unified wireless network testbed for education and research," in *Microelectronic Systems Education, 2007. MSE'07. IEEE International Conference on*. IEEE, 2007, pp. 53–54.

[10] A. F. Molisch, *Wireless communications 2nd ed.* Wiley, 2010.

[11] J. Karedal, N. Czink, A. Paier, F. Tufvesson, and A. F. Molisch, "Path loss modeling for vehicle-to-vehicle communications," *Vehicular Technology, IEEE Transactions on*, vol. 60, no. 1, pp. 323–328, 2011.

[12] M. Boban, T. T. Vinhoza, M. Ferreira, J. Barros, and O. K. Tonguz, "Impact of vehicles as obstacles in vehicular ad hoc networks," *Selected Areas in Communications, IEEE Journal on*, vol. 29, no. 1, pp. 15–28, 2011.

[13] J. Kunisch and J. Pamp, "Wideband car-to-car radio channel measurements and model at 5.9 GHz," in *Vehicular Technology Conference, 2008. VTC 2008-Fall. IEEE 68th*. IEEE, 2008, pp. 1–5.

[14] M. Gudmundson, "Correlation model for shadow fading in mobile radio systems," *Electronics letters*, vol. 27, no. 23, pp. 2145–2146, 1991.

[15] K. P. Burnham and D. R. Anderson, *Model selection and multi-model inference: a practical information-theoretic approach*. Springer, 2002.

[16] U. G. Schuster and H. Bolcskei, "Ultrawideband channel modeling on the basis of information-theoretic criteria," *Wireless Communications, IEEE Transactions on*, vol. 6, no. 7, pp. 2464–2475, 2007.

[17] I. Sen and D. W. Matolak, "Vehicle–vehicle channel models for the 5-GHz band," *Intelligent Transportation Systems, IEEE Transactions on*, vol. 9, no. 2, pp. 235–245, 2008.

[18] L. Cheng, B. E. Henty, D. D. Stancil, F. Bai, and P. Mudalige, "Mobile vehicle-to-vehicle narrow-band channel measurement and characterization of the 5.9 GHz dedicated short range communication (DSRC) frequency band," *Selected Areas in Communications, IEEE Journal on*, vol. 25, no. 8, pp. 1501–1516, 2007.

[19] M. Yacoub, G. Fraidenraich *et al.*, "A simple accurate method for generating autocorrelated Nakagami-m envelope sequences," *Communications Letters, IEEE*, vol. 11, no. 3, pp. 231–233, 2007.

[20] A. Laourine, M.-S. Alouini, S. Affes, and A. Stéphenne, "On the performance analysis of composite multipath/shadowing channels using the G-distribution," *Communications, IEEE Transactions on*, vol. 57, no. 4, pp. 1162–1170, 2009.